A&A 450, 117–128 (2006)
DOI: 10.1051/0004-6361:20054297

Astronomy & Astrophysics

X-ray luminosity function of faint point sources in the Milky Way

S. Sazonov[1,2], M. Revnivtsev[1,2], M. Gilfanov[1,2], E. Churazov[1,2], and R. Sunyaev[1,2]

[1] Max-Planck-Institut für Astrophysik, Karl-Schwarzschild-Str. 1, 85740 Garching bei München, Germany
e-mail: sazonov@mpa-garching.mpg.de
[2] Space Research Institute, Russian Academy of Sciences, Profsoyuznaya 84/32, 117997 Moscow, Russia

Received 3 October 2005 / Accepted 15 December 2005

ABSTRACT

We assessed the contribution to the X-ray (above 2 keV) luminosity of the Milky Way by different classes of low-mass binary systems and single stars. We began by using the RXTE Slew Survey of the sky at $|b| > 10^\circ$ to construct an X-ray luminosity function (XLF) of nearby X-ray sources in the range 10^{30} erg s^{-1} $< L_x < 10^{34}$ erg s^{-1} (where L_x is the luminosity over 2–10 keV), occupied by coronally active binaries (ABs) and cataclysmic variables (CVs). We then extended this XLF down to $L_x \sim 10^{27.5}$ erg s^{-1} using the Rosat All-Sky Survey in soft X-rays and available information on the 0.1–10 keV spectra of typical sources. We found that the local cumulative X-ray (2–10 keV) emissivities (per unit stellar mass) of ABs and CVs are $(2.0 \pm 0.8) \times 10^{27}$ and $(1.1 \pm 0.3) \times 10^{27}$ erg s^{-1} $M_\odot^{-1}$, respectively. In addition to ABs and CVs representing old stellar populations, young stars locally emit $(1.5 \pm 0.4) \times 10^{27}$ erg s^{-1} $M_\odot^{-1}$. Finally to the XLF of ABs and CVs we attached a high luminosity branch (up to $\sim 10^{39}$ erg s^{-1}) composed of neutron-star and black-hole low-mass X-ray binaries (LMXBs), derived in previous work. The combined XLF covers $\sim$12 orders of magnitude in luminosity. The estimated combined contribution of ABs and CVs to the 2–10 keV luminosity of the Milky Way is $\sim 2 \times 10^{38}$ erg s^{-1}, or $\sim$3% of the integral luminosity of LMXBs averaged over nearby galaxies. The XLF obtained in this work is used elsewhere to assess the contribution of point sources to the Galactic ridge X-ray emission.

Key words. stars: luminosity function, mass function – Galaxy: structure – X-rays: binaries – X-rays: galaxies – X-rays: stars

1. Introduction

X-ray (above 2 keV) emission is a ubiquitous property of different classes of low-mass close binaries, ranging in order of increasing luminosity from chromospherically and coronally active binaries (ABs) through cataclysmic variables (CVs, magnetic and non-magnetic) and related white-dwarf accretors (symbiotic stars) to neutron-star and black-hole binaries (LMXBs). Although each of these classes has been thoroughly investigated for decades, there remains significant uncertainty as regards the contribution of ABs and CVs, both cumulative and as a function of luminosity, to the integral X-ray luminosity of the Galaxy. On the other hand, the luminosity function (XLF) of LMXBs has been measured with good precision for the Milky Way and nearby galaxies (Grimm et al. 2002; Gilfanov 2004).

There are several important astrophysical problems urging a detailed study of the XLF of ABs and CVs. First, there is the long-standing puzzle of the origin of the Galactic ridge X-ray emission (e.g. Worrall et al. 1982; Warwick et al. 1985). Although there were early suggestions that this apparently diffuse X-ray emission might be composed of thousands and millions of CVs and ABs (Worrall & Marshall 1983; Ottmann & Schmitt 1992; Mukai & Shiokawa 1993), recent deep surveys by Chandra and XMM-Newton in the Galactic plane and in the Galactic center region resolved only ∼10–30% of the ridge emission (above 2 keV) into point sources (Muno et al. 2004; Ebisawa et al. 2005; Hands et al. 2004), leaving the question open as to what fraction of the unresolved emission is truly diffuse.

Secondly, with the advent of Chandra it has become possible to obtain high-quality X-ray maps of nearby elliptical galaxies and resolve individual LMXBs on them. The underlying diffuse emission is usually attributed to the hot (∼0.5 keV) interstellar gas. However, in gas-poor galaxies unresolved point X-ray sources associated with the old stellar population may contribute significantly to or even dominate the apparently diffuse emission, especially at high energies (e.g. Canizares et al. 1987; Matsumoto et al. 1997; Irwin et al. 2003). The interpretation of the X-ray observations of gas-poor ellipticals thus critically depends on our knowledge of the XLF of low-mass binaries in these galaxies, which is expected to resemble the XLF of ABs, CVs, and LMXBs in our Galaxy scaled by the stellar mass.

With the above motivation in mind, we constructed a combined XLF of ABs, CVs, and LMXBs covering the very broad luminosity range from $L_x \sim 10^{27.5}$ to $\sim 10^{39}$ erg s^{-1}, where L_x is the luminosity in the 2–10 keV band. Since these classes of objects represent old stellar populations (in particular ABs maintain high levels of activity throughout their lives due to

tidal locking of rapid stellar rotation), their XLF normalized to the stellar mass is not expected to vary significantly across the Galaxy and also between different types of galaxies. This has already been observationally demonstrated for LMXBs (Gilfanov 2004). In contrast, the statistics of young coronal stars (YSs), another abundant class of low-luminosity X-ray sources (see Güdel 2004, for a review), is expected to be governed by local star formation history, so that an XLF constructed for this class of sources in the solar neighborhood may not be representative of other parts of the Galaxy and other galaxies. It will be shown below that YSs produce ∼30% of the integral 2–10 keV emissivity in the solar neighborhood.

Our assessment of source space densities at $L_x < 10^{34}$ erg s^{-1} is based on the RXTE Slew Survey (Revnivtsev et al. 2004, hereafter R04) and Rosat All-Sky Survey (`http://www.xray.mpe.mpg.de/cgi-bin/rosat/rosat-survey`; Voges et al. 1999). In the latter case we also employed spectral information from various X-ray missions to convert the derived XLF from a soft X-ray band to the standard X-ray band. The high-luminosity ($L_x > 10^{34}$ erg s^{-1}) branch of the XLF is adopted from previous work of Gilfanov (2004).

2. Medium luminosity range: RXTE Slew Survey

Recently, a serendipitous survey of the whole sky in the 3–20 keV energy band was performed based on slew observations with the PCA instrument on the RXTE spacecraft (RXTE Slew Survey, or XSS), and a source catalog at high Galactic latitude ($|b| > 10°$) was produced (R04). The survey achieved a flux limit of 2.5×10^{-11} erg cm^{-2} s^{-1} (3–20 keV) or better for 90% of the $|b| > 10°$ sky.

The majority of the 294 detected XSS sources have been identified with extragalactic objects, 60 sources have been identified with objects in the Galaxy, while 21 sources still remain unidentified. The identified Galactic sample includes 14 LMXBs and HMXBs, which were not considered in this study. We also excluded from consideration: 4 star forming complexes with multiple X-ray sources as unresolvable by RXTE (Orion, Chamaeleon 1, Chamaeleon 2, and ρ Ophiuchi), the hot supergiant star ζ Ori as also belonging to the Orion complex, the unresolved globular cluster NGC 6397, and supernova remnant SN 1006 as an extended X-ray source. This left us with a total of 40 identified ABs (including 2 candidates, see below) and CVs. Of these we additionally excluded 10 sources for either of the following reasons: 1) the source is not detectable on the average XSS map and was originally included in the XSS catalog based on its transient detection, 2) the source was the target of pointed RXTE observations and would not have been detected in slew observations otherwise.

We thus obtained a sample (see Table 1) of 30 ABs and CVs detected with $\geq 4\sigma$ significance on the average XSS sky map (3–20 keV). This sample is well suited for statistical studies.

For each source, the XSS catalog provides RXTE/PCA count rates in the 3–8 keV and 8–20 keV bands. We found published distances to all sources except for the intermediate polar V1025 Cen (for which we assumed a distance of 400 pc, a value typical of the intermediate polars in our sample), the polar CD Ind (for which we used the available lower limit) and the source XSS J17309−0552 discussed below. Parallax measurements, in many cases adopted directly from the Hipparcos or Tycho catalog, were used wherever available. For XSS J17309−0552/RXS J173021.5−055933, a recently discovered intermediate polar (Gänsicke et al. 2005), we estimated the distance using available information about the secondary star (Gänsicke et al. 2005). Specifically, this GV star contributes ∼15% to the R-band flux of the binary. Given the system's visual magnitude ($R_V = 15.4$) and interstellar extinction toward it [$E(B-V) \sim 0.45$], and assuming that the secondary is on the main sequence, one finds a distance ∼2300–3100 pc. However, the very long orbital period of the binary (15.4 h) implies that the Roche-lobe filling secondary is evolved (e.g. Smith & Dhillon 1998). This yields a more likely distance of ∼3300 pc, which we adopted.

Using the distance estimates and measured source count rates in the 3–8 keV and 3–20 keV bands, we determined source luminosities in the 2–10 keV (L_x) and 3–20 keV (L_h) bands, respectively. A Crab-like spectrum was assumed for this calculation, which is expected to ensure reasonable accuracy of energy flux estimation for our sources, given their measured hardness ratios (8–20 keV counts over 3–8 keV counts). We note that the quoted luminosities are observed ones, i.e. they were not corrected for any absorption intrinsic to the sources. The interstellar absorption toward our (high Galactic latitude) sources is not expected to have a significant effect on the RXTE measured fluxes. This is true even in the case of XY Ari, the only source in our sample known to be located behind a molecular cloud, for which we estimated a line-of-sight absorption of $N_H \sim 2 \times 10^{22}$ cm^{-2} from the measured visual extinction $A_V \sim 11.5$ (Littlefair et al. 2001). Similarly the uncertainty in source distances is unlikely to significantly affect the statistical results presented below.

Our XSS sample includes 6 known or suspected ABs and 24 known CVs. Among the former there are 3 RS CVn binaries, the prototype Algol system (β Per), and 2 late-type main-sequence stars (HD 125599 and HD 130693) that we consider candidate ABs based on their optical spectral class, X-ray luminosities, and relative X-ray softness compared to CVs. The CV subsample includes 4 non-magnetic CVs (dwarf novae), 19 magnetic CVs (6 polars and 13 intermediate polars) and 1 symbiotic star.

In Fig. 1 we plot the XSS hardness ratio as a function of luminosity for our identified sample. One can see that, as expected, the ABs have softer spectra than do the CVs. As regards the latter, the intermediate polars and the only symbiotic star in our sample tend to have somewhat harder spectra than the polars and dwarf novae.

Despite the relatively small size of our sample, it can be used to construct an XLF, since it covers 4 orders of magnitude in luminosity (from ∼10^{30} to ∼10^{34} erg s^{-1}) and is derived from a flux-limited survey with a direction-dependent sensitivity limit. As usual for such surveys, one can readily estimate the space density of sources in a given luminosity interval using the $1/V_{max}$ method (Schmidt 1968). To this end, we used the XSS exposure map presented in R04, which yields the space volume probed by the survey for a given source luminosity.

Table 1. XSS sources identified with ABs and CVs.

XSS source (J2000.0)	Name	Class[a]	D[b] pc	$L_{\rm h}^{c}$ erg/s	$L_{\rm x}^{d}$ erg/s	Hardness ratio	$1/V_{\rm gen}$ pc^{-3}
02290−6931	RBS 324	P	250 [1]	31.88	31.70	0.41 ± 0.25	4.9×10^{-8}
02569+1931	XY Ari	IP	270 [2]	32.43	32.12	0.88 ± 0.42	1.2×10^{-8}
03089+4101	β Per	AL	28 [3]	30.91	30.77	0.28 ± 0.06	8.9×10^{-7}
03385+0029	V711 Tau	RS	29 [3]	30.23	30.15	0.10 ± 0.19	8.2×10^{-6}
05019+2444	V1062 Tau	IP	1100 [4]	33.77	33.51	0.69 ± 0.12	1.2×10^{-9}
05295−3252	TV Col	IP	370 [5]	33.08	32.80	0.77 ± 0.09	3.1×10^{-9}
05432−4116	TX Col	IP	500 [4]	32.71	32.50	0.52 ± 0.21	6.3×10^{-9}
05450+6049	BY Cam	P	190 [6]	31.96	31.74	0.55 ± 0.24	3.9×10^{-8}
06132+4755	SS Aur	DN	280 [7]	32.17	31.97	0.48 ± 0.24	2.2×10^{-8}
07514+1442	PQ Gem	IP	400 [4]	32.79	32.54	0.68 ± 0.20	5.3×10^{-9}
08010+6241	HT Cam	IP	400 [8]	32.72	32.46	0.70 ± 0.29	6.2×10^{-9}
08142+6231	SU Uma	DN	260 [7]	32.16	31.99	0.37 ± 0.17	2.3×10^{-8}
11474+7143	DO Dra	IP	155 [4]	32.02	31.78	0.62 ± 0.10	3.3×10^{-8}
12392−3820	V1025 Cen	IP	400 [9]	32.36	32.19	0.37 ± 0.14	1.4×10^{-8}
12529−2911	EX Hya	IP	65[10]	31.79	31.62	0.40 ± 0.02	6.2×10^{-8}
13355+3714	BH CVn	RS	45 [3]	31.15	31.07	0.11 ± 0.11	4.2×10^{-7}
14100−4500	V834 Cen	P	150[11]	31.72	31.48	0.61 ± 0.12	7.6×10^{-8}
14241−4803	HD125599[e]	?	90 [3]	30.72	30.62	0.15 ± 0.15	1.6×10^{-6}
14527−2414	HD130693[f]	?	27[12]	30.07	29.93	0.28 ± 0.08	1.4×10^{-5}
16167−2817	V893 Sco	DN	150 [7]	32.10	31.92	0.40 ± 0.08	2.7×10^{-8}
17309−0552	1RXS J173021.5-055933	IP	3300[13]	34.28	34.06	0.54 ± 0.29	8.1×10^{-10}
17597+0821	V2301 Oph	P	150[14]	31.90	31.67	0.56 ± 0.10	4.6×10^{-8}
18080+0622	V426 Oph	DN	200[15]	32.07	31.85	0.56 ± 0.25	2.9×10^{-8}
18164+5004	AM Her	P	79 [7]	31.77	31.50	0.74 ± 0.05	6.6×10^{-8}
18553−3111	V1223 Sgr	IP	510[16]	33.73	33.45	0.76 ± 0.02	1.2×10^{-9}
19243+5041	CH Cyg	SS	250[17]	32.26	31.87	1.25 ± 0.26	1.8×10^{-8}
21155−5836	CD Ind	P	250[18]	31.90	31.64	0.70 ± 0.24	4.6×10^{-8}
22178−0822	FO Aqr	IP	300 [4]	32.85	32.53	0.94 ± 0.09	4.7×10^{-9}
22526+1650	IM Peg	RS	97 [3]	31.65	31.46	0.42 ± 0.03	9.3×10^{-8}
22551−0309	AO Psc	IP	250 [4]	32.57	32.33	0.60 ± 0.10	8.6×10^{-9}

[a] Class: RS – RS CVn; AL – Algol; DN – dwarf nova; P – polar; IP – intermediate polar; SS – symbiotic star.
[b] Reference for distance: 1 – Schwope et al. (2002); 2 – Littlefair et al. (2001); 3 – Hipparcos; 4 – Patterson (1994); 5 – McArthur et al. (2001); 6 – Warner (1995); 7 – Thorstensen (2003); 8 – Tovmassian (1998); 9 – assumed; 10 – Eisenbart et al. (2002); 11 – Araujo-Betancor et al. (2005); 12 – Tycho; 13 – based on Gänsicke et al. (2005), see main text; 14 – Silber et al. (1994); 15 – Hessman (1998); 16 – Beuermann et al. (2004); 17 – Sokoloski & Kenyon (2003); 18 – lower limit (The MSSL Polar Page, `http://www.mssl.ucl.ac.uk/www_astro/gal/polar.html`).
[c] Log of 3–20 keV luminosity.
[d] Log of 2–10 keV luminosity.
[e] Bright (V = 8.5) F7/8V star associated with the bright ROSAT source 1RXS J142148.7−480420.
[f] Bright (V = 8.2) G6V star associated with the bright ROSAT source 1RXS J145017.6−242558 = RBS 1436 (Schwope et al. 2000).

To take into account the fact that the studied classes of sources are concentrated toward the Galactic plane, we assumed that the space density of ABs and CVs declines with height as $\exp(-z/h)$, where $h = 150$ pc. This adopted scale height is appropriate for the CVs (e.g. Patterson 1984), while the inferred space density of ABs is only weakly sensitive to the assumed value of h, since ABs are detectable within ∼100 pc of the Sun in the XSS. Note that the Galactocentric dependence is not important for us since our studied objects are located within ∼1 kpc of the Sun. We therefore weighted the standard $\delta V_{\rm max}$ volume found for each small solid angle $\delta\Omega$ (at Galactic latitude b) of the survey by the space density of sources integrated over $\delta\Omega$ and over distance from 0 to $d_{\rm max}$, the maximum distance at which a given XSS source is detectable (Tinney et al. 1993; Schwope et al. 2002):

$$\delta V_{\rm gen} = \delta\Omega \frac{h^3}{\sin^3 b}\left[2 - \left(\xi^2 + 2\xi + 2\right)\mathrm{e}^{-\xi}\right], \quad (1)$$

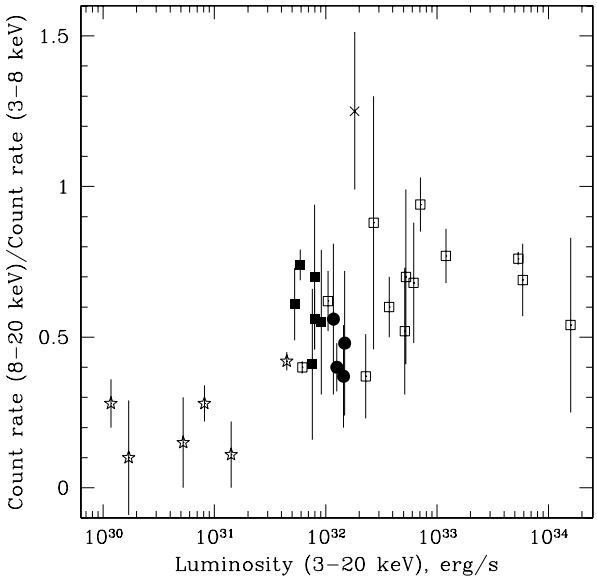

Fig. 1. The RXTE/PCA hardness ratio vs. 3–20 keV luminosity for XSS sources identified with ABs and CVs: open stars – ABs, filled circles – dwarf novae, filled squares – polars, open squares – intermediate polars, the cross – a symbiotic star.

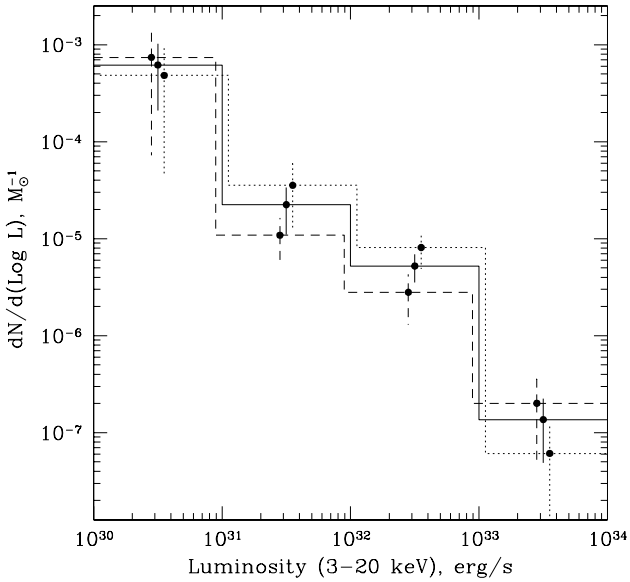

Fig. 2. Differential 3–20 keV luminosity function of ABs and CVs derived from the XSS. Solid, dotted, and dashed histograms and error bars show the XLFs for the whole, northern, and southern sky, respectively. The northern and southern XLFs are slightly shifted along the luminosity axis for better visibility.

where $\xi = d_{\max} \sin b/h$. Each sampled source then contributes $1/\sum \delta V_{\rm gen}$ to the estimated space density and $1/(\sum \delta V_{\rm gen})^2$ to the associated variance, where the sum is taken over the total solid angle of the survey.

We show in Fig. 2 the resulting differential XLF of ABs and CVs in the 3–20 keV energy band, covering the luminosity range 10^{30}–10^{34} erg s^{-1}. This XLF was normalized to the local stellar mass density, assumed to be 0.04 $M_\odot$ pc^{-3} throughout the paper (Jahreiß & Wielen 1997; Robin et al. 2003). The values of $1/V_{\rm gen}$ for individual XSS sources are given in Table 1. Note that we excluded the intermediate polar XSS J17309−0552/RXS J173021.5−055933 from the XLF construction since its inferred X-ray luminosity exceeds 10^{34} erg s^{-1}, making it the only source with such high luminosity in our sample.

It is necessary to check whether the derived XLF suffers from incompleteness of the input sample. There are in fact 18 unidentified XSS sources[1] – see Table 2. Although, we suspect (see R04) that most of these sources are active galactic nuclei, this has not yet been verified and therefore we must take this additional sample into account.

We expect our identified sample to be highly complete at $L_{\rm h} \gtrsim 10^{30}$ erg s^{-1} with respect to ABs and other types of coronal stars for the following reasons. First, it is very unlikely that more than ∼1–2 of the 13 unidentified XSS sources (see Table 2) for which there is no obvious bright counterpart in the Rosat All-Sky Survey (RASS) are ABs or YSs, because coronal X-ray sources are relatively soft. To illustrate this point we plot in Fig. 3 the ratio of the ROSAT/PSPC count rate (0.1–2.4 keV) to the RXTE/PCA count rate (3–20 keV) as a function of the latter for our identified and unidentified sources. For the 13 XSS sources without a firm RASS counterpart, an upper limit is shown that was derived from the ROSAT/PSPC count rate of the brightest RASS source within the XSS localization region (typically 0.5–1° in radius, R04). The unidentified XSS sources without a bright RASS counterpart are apparently hard X-ray sources compared to the identified ABs. It is

Table 2. Unidentified XSS sources.

XSS source (J2000.0)	Hardness ratio	Counterpart from RASS Bright Source Catalog
00050−6904	0.46 ± 0.11	
00564+4548	0.52 ± 0.08	1RXS J005528.0+461143
02087−7418	0.86 ± 0.23	
05188+1823	0.70 ± 0.34	
12270−4859	0.52 ± 0.13	1RXS J122758.8−485343
13563−7342	0.46 ± 0.26	
14101−2936	1.19 ± 0.47	
14138−4022	0.46 ± 0.23	
14239−3800	0.51 ± 0.21	1RXS J142149.8−380901
14353−3557	0.59 ± 0.33	
14495−4005	0.45 ± 0.15	
15360−4118	0.63 ± 0.29	
16049−7302	0.76 ± 0.32	
16537−1905	0.70 ± 0.24	
17223−7301	0.37 ± 0.27	1RXS J171850.0−732527[a]
17576−4534	0.63 ± 0.30	
18486−2649	0.43 ± 0.24	
19303−7950	0.49 ± 0.24	1RXS J194944.6−794519

[a] Possibly associated with star Tyc 9288-744-1 (V = 9.8).

[1] Note that Sazonov & Revnivtsev (2004) listed 35 unidentified XSS sources, but 5 of those sources were transiently detected and another 12 have been identified since publication.

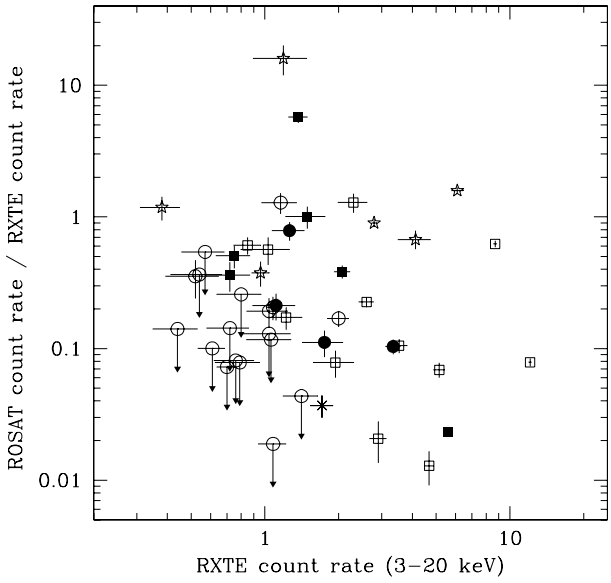

Fig. 3. Ratio of the ROSAT/PSPC count rate (0.1–2.4 keV) to the RXTE/PCA count rate (3–20 keV) for the identified and unidentified XSS sources. Identified sources of different classes are denoted by the same symbols as in Fig. 1, and unidentified sources are shown by empty circles. The ROSAT count rates and upper limits are adopted from the RASS Bright Source Catalog (Voges et al. 1999) and RASS Faint Source Catalog, except for V1062 Tau where we used pointed ROSAT/PSPC observations. The source XY Ari is not shown since its observed soft X-ray flux is strongly diminished by absorption in an intervening molecular cloud (Littlefair et al. 2001).

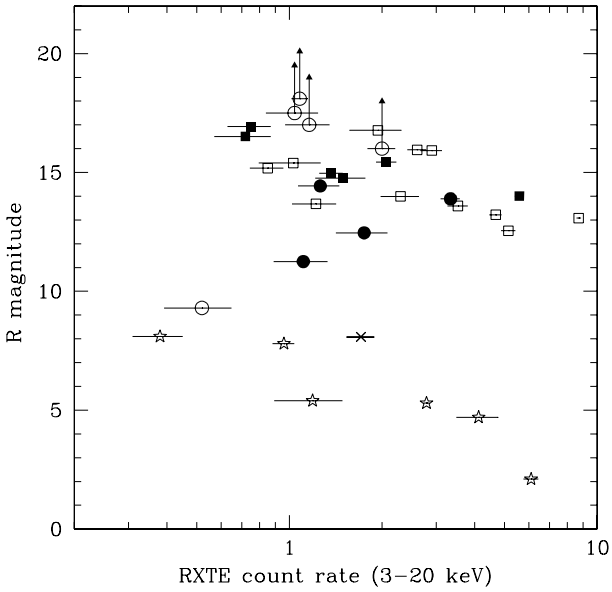

Fig. 4. The *R*-band visual magnitude vs. RXTE/PCA count rate for the identified XSS sources and 5 unidentified XSS sources with a firm RASS counterpart. Identified sources of different classes are denoted by the same symbols as in Fig. 1, unidentified sources are shown by empty circles, *R* magnitudes and lower limits are adopted from the USNO-B1.0 Catalog. The XSS source XY Ari is not shown since its optical spectrum is strongly reddened by absorption within a molecular cloud (Littlefair et al. 2001).

important to note that the presented XSS source fluxes are averages over multiple RXTE/PCA observations separated by up to several years, hence it can be expected that these fluxes are not strongly biased by individual X-ray flares relative to the level of source persistent activity.

Secondly, for the 5 unidentified XSS sources reliably associated with an RASS source (see Table 2), one can search for a bright star inside the ROSAT localization region, typically less than 30 arcsec in radius. A source with a 3–20 keV luminosity of 10^{30}–$10^{31.5}$ erg s^{-1} (the higher value is quite extreme for coronal sources) would typically be detectable in the XSS out to ∼20–100 pc. Stars exhibiting such high levels of coronal activity are rapidly rotating (usually in short-period binaries) main-sequence or evolved late-type stars, with $M_V \lesssim 6$ (see e.g. Singh et al. 1996; Makarov 2003). Therefore, if any of the unidentified XSS sources were a high luminosity coronal source, we would expect to find a star that is brighter than $V \sim 11$ in the ROSAT localization region. Searches in the Hipparcos and Tycho catalogs revealed only one such bright star, a possible counterpart to XSS J17223−7301/1RXS J171850.0−732527 (see Table 2). Should this association be confirmed, it will not significantly change our estimate of the space density of ABs. Figure 4 illustrates the above argument by showing the *R*-band visual magnitudes (or lower limits) vs. the RXTE/PCA count rate for identifed XSS sources and for the 5 unidentified XSS sources with an RASS counterpart. One can see that the optical counterparts of the unidentified XSS sources (except for XSS J17223−7301 mentioned above) are much dimmer than expected for coronal sources.

On the other hand, since CVs can be undetectable in the RASS due to their hard spectra (see Fig. 3) and can also be inconspicuous optically (see Fig. 4), it is possible that some of the unidentified XSS sources belong to this class. There is an additional possibility of testing the XLF obtained. Our identified sample is highly complete in the northern hemisphere: there are 16 identified and 2 unidentified sources at $\delta > 0$. This contrasts with the southern hemisphere, where there are 13 (excluding the high-luminosity XSS J17309−0552/RXS J173021.5−055933) identified vs. 16 unidentified sources. It is therefore worth comparing XLFs determined from the northern and southern subsamples. As shown in Fig. 2, the resulting XLFs agree with each other and with the all-sky XLF within the uncertainties, although there is a hint that the southern sample of CVs may be somewhat incomplete.

We conclude that we may be underestimating the combined XLF of ABs and CVs at $L_h \gtrsim 10^{31}$ erg s^{-1}, since several unidentified CVs may remain in the XSS catalog. The associated systematic uncertainty is unlikely to exceed 50% though.

3. Low luminosity range: Rosat All-Sky Survey

The weakest X-ray source (a candidate AB) in the XSS sample has a luminosity $L_x \approx 10^{30}$ erg s^{-1} in the 2–10 keV band. To extend our study to $L_x < 10^{30}$ erg s^{-1}, a large-area survey is necessary that is more sensitive than the XSS and has highly complete source identification. Since no such survey has

Table 3. Space densities of soft X-ray active stars derived from the RASS.

$\log L_s$	D	All stars		ABs		Catalog
	pc	Number	Density, pc^{-3}	Number	Density, pc^{-3}	
31.0–31.5	50	7	$(1.3 \pm 0.5) \times 10^{-5}$	6	$(1.1 \pm 0.5) \times 10^{-5}$	M03
30.5–31.0	50	18	$(3.4 \pm 0.8) \times 10^{-5}$	12	$(2.3 \pm 0.7) \times 10^{-5}$	M03
30.0–30.5	50	73	$(1.5 \pm 0.2) \times 10^{-4}$	24	$(4.6 \pm 0.9) \times 10^{-5}$	M03
29.5–30.0	25	31	$(4.7 \pm 0.9) \times 10^{-4}$	9	$(1.4 \pm 0.5) \times 10^{-4}$	H99
...	15			3	$(2.1 \pm 1.2) \times 10^{-4}$	H99
29.0–29.5	25	96	$(1.5 \pm 0.2) \times 10^{-3}$	11	$(1.7 \pm 0.5) \times 10^{-4}$	H99
...	15			7	$(5.0 \pm 1.9) \times 10^{-4}$	H99
28.5–29.0	25	131	$(2.0 \pm 0.2) \times 10^{-3}$	5	$(8.0 \pm 3.0) \times 10^{-5}$	H99
...	15			3	$(2.1 \pm 1.2) \times 10^{-4}$	H99
28.0–28.5	20	132	$(3.9 \pm 0.3) \times 10^{-3}$			H99
27.5–28.0	11	48	$(8.6 \pm 1.2) \times 10^{-3}$			H99
27.0–27.5	6	18	$(2.0 \pm 0.5) \times 10^{-2}$			H99

been performed so far in the standard (2–10 keV) or similar X-ray band, we considered different options. Taking into account the fact that coronal stars with $L_x < 10^{30}$ erg s^{-1} are characterized by soft spectra, we decided to use the Rosat All-Sky Survey. Furthemore, by using spectral data from different X-ray missions, it proved possible to convert the space density of ROSAT sources detected in the 0.1–2.4 keV band to harder X-ray bands.

Our analysis was based on two published catalogs derived from the RASS: the catalog of the 100 most luminous X-ray stars within 50 pc of the Sun (Makarov 2003, hereafter M03) and the RASS catalog of the nearby stars (Hünsch et al. 1999, hereafter H99). The first catalog includes all stars with 0.1–2.4 keV luminosity (L_s) higher than 9.8×10^{29} erg s^{-1}. The second catalog includes all objects from the Third Catalog of Nearby Stars (Gliese & Jahreiß 1991) that were detected in the RASS. Both catalogs are well suited for our statistical study since they are expected to be highly complete and since they provide accurate parallax distances for the sources.

The ABs of RS CVn, BY Dra, Algol, W Uma and other types (mostly of the first two types) make up 43% of the M03 sample. Another 42% consist mostly of pre-main-sequence and young main-sequence stars, while 15% of the stars are not classified. We therefore determined the space density of all sources and did it separately for ABs. Since the M03 is volume-limited, the source space density can be found as

$$\rho = \frac{N}{(4\pi/3)D^3}, \qquad (2)$$

where $D = 50$ pc for the M03 sample. We ignored the small effect of decreasing space density with height above the Galactic plane. The resulting space densities for 3 luminosity intervals are given in Table 3. Note that, although we ignored the small number of unknown-type sources when estimating the space density of ABs, this cannot affect the result significantly.

The H99 catalog is expected to be highly complete within 25 pc of the Sun with respect to X-ray stars with $L_s > 1.5 \times 10^{28}$ erg s^{-1}. This follows from the fact that for 97% of the sky an exposure of 100 s or longer was achieved in the RASS (Voges et al. 1999), which for coronally active stars typically corresponds to a 0.1–2.4 keV flux limit of $\sim 2 \times 10^{-13}$ erg cm^{-2} s^{-1} (Hünsch et al. 1999). Given this flux limit one can readily find a distance D within which the H99 catalog should be complete for a given limiting luminosity. One can then again apply Eq. (2) to estimate the space density of X-ray stars with luminosities exceeding this limit within distance D.

To separate ABs from other sources we need information about source classes, which is not provided by H99. We thus cross-correlated the H99 sample with published catalogs of chromospherically active binaries (Strassmeier et al. 1993; Karataş et al. 2004). A few additional RS CVn and W Uma systems were found by cross-correlating the H99 catalog with the General Catalog of Variable Stars (Samus et al. 2004). Since it is possible that these catalogs are not complete at low luminosities, we resticted our analysis to ABs with $L_s > 10^{28.5}$ erg s^{-1}. We also compared the space density of ABs within 25 pc with that within 15 pc. Table 3 provides space densities for X-ray stars in a number of luminosity intervals, as derived from the H99 sample.

Combining the results from the M03 and H99 samples we obtained the differential soft X-ray luminosity function of nearby low-luminosity sources shown in Fig. 5. One can see that between $L_s \sim 10^{30.5}$ and $\sim 10^{31.5}$ erg s^{-1}, ABs dominate the local X-ray source population. At lower luminosities, the fraction of YSs (and normal, Sun-like stars at the lower end of the luminosity function) becomes progressively higher, although the somewhat higher space density of ABs found within $D = 15$ pc compared to $D = 25$ pc may indicate that the catalogs of ABs start to be incomplete at $L_s \lesssim 10^{29.5}$ erg s^{-1} within the larger volume.

Our analysis implies that the local space density of ABs with $L_s > 10^{28.5}$ erg s^{-1} is $(4.7 \pm 0.8) \times 10^{-4}$ pc^{-3} (using $D = 25$ pc for the H99 sample), in satisfactory agreement with the estimate based on the Einstein Extended Medium Sensitivity Survey of $(2.9 \pm 0.6) \times 10^{-4}$ pc^{-3} (Fleming et al. 1989; Ottmann & Schmitt 1992). It also follows from the above

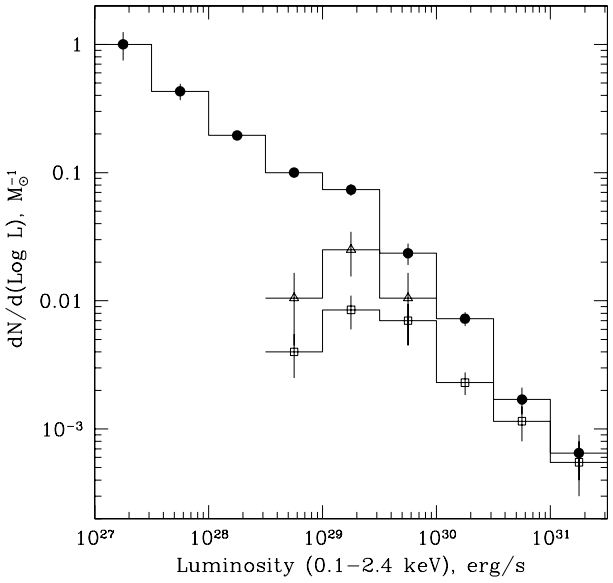

Fig. 5. Differential soft X-ray luminosity function of stars in the solar neighborhood derived from the RASS. The filled circles show the XLF of all stars, and the open squares show the XLF of ABs within 50 pc of the Sun. For three low-luminosity bins the XLF of ABs within 15 pc of the Sun is also shown (triangles).

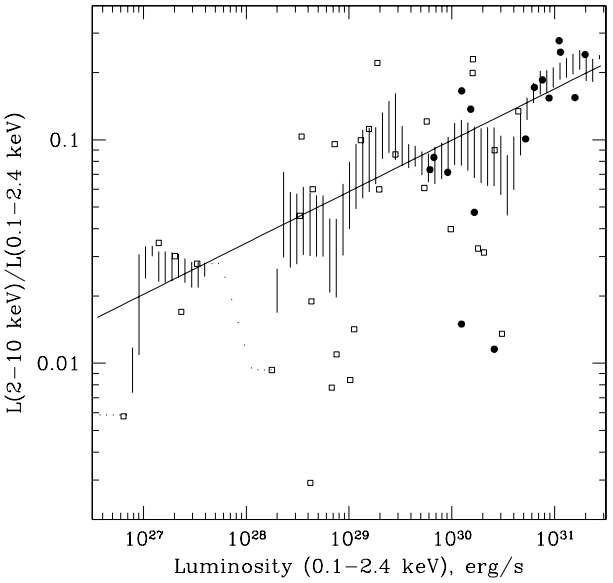

Fig. 6. Ratio of luminosities in the 2–10 keV and 0.1–2.4 keV energy bands as a function of soft X-ray luminosity for RASS sources, estimated from ASCA or Chandra spectra. Solid symbols denote ABs and open symbols other coronal stars. Also shown (shaded region) is the 1σ confidence region (determined by the scatter of individual measurements around the mean value) for a sliding-window average ($\Delta \log L_s = 0.5$) of the presented data points, and the power-law approximation (solid line) to this average given by Eq. (3).

analysis that stars with $L_s < 10^{29}$ erg s^{-1} produce less than 20% of the total local soft X-ray emissivity (see Table 4). We point out that the soft X-ray luminosity function shown in Fig. 5 extends from the most luminous coronal stars ($L_s \sim 10^{31.5}$ erg s^{-1}) down to Sun-like stars ($L_s \sim 10^{27}$ erg s^{-1}).

3.1. Conversion from the ROSAT energy band to the standard X-ray band

Conversion of the soft X-ray luminosity function obtained above to the 2–10 keV energy band requires knowledge of the source spectra. Since the majority of RASS sources used in our analysis have not been observed in the standard X-ray band, we are bound to rely on a representative set of sources for which broad-band spectra are available. To this end we selected X-ray observations from public archives, of sufficiently good quality for spectral analysis, for 22 sources from the M03 sample and 25 sources from the H99 sample. All observations were performed by ASCA, except for the star GJ 1245 observed by Chandra. The ASCA and Chandra data were then processed by standard tasks of HEASOFT and CIAO packages according to recipes of the Guest Observer Facilities (`http://legacy.gsfc.nasa.gov/docs/asca/ascagof.html` and `http://cxc.harvard.edu/ciao/`).

In the 0.5–10 keV band the moderate resolution spectra of all selected sources are well fit by a broken power law with the break energy and lower-energy photon index fixed at 0.8 keV and 1.5, respectively. The high-energy photon index was a free parameter in our analysis and we found best-fit values for it in the range ∼3 to ∼5 for different sources. This simple empirical model mimics reasonably well the actual multi-temperature emission spectrum (e.g. Schmitt et al. 1990; Dempsey et al. 1993; Güdel 2004) dominated by strong blended line emission below ∼0.8 keV. From the best-fit model we found the ratio for each source of its luminosity in the 2–10 keV band to that in the 0.5–2 keV band.

We then went on to convert L (0.5–2 keV) to L_s, luminosity in the ROSAT (0.1–2.4 keV) band, assuming $L(0.5\text{–}2\ \text{keV})/L_s \sim 0.7$, a ratio typical of the coronal stars observed by Einstein and ROSAT (Fleming et al. 1995). The resulting values of L_x/L_s are plotted as a function of L_s in Fig. 6 for our spectral sample of sources. In most cases the L_s value determined from ASCA or Chandra observations differs by less than a factor of 2 from the soft X-ray luminosity directly measured by ROSAT at a different epoch.

Figure 6 confirms the well-known trend of the hardening of stellar coronal X-ray emission with increasing luminosity (e.g. Schmitt et al. 1990; Güdel 2004). It also demonstrates that ABs do not distinguish themselves spectrally from YSs with similar luminosities. Averaging the ratios L_x/L_s for individual sources in a sliding window of width $\Delta \log L_s = 0.5$ led to the result shown by the shaded region in Fig. 6, which reflects the uncertainty in $\langle L_x/L_s \rangle$ due to the scatter of individual L_x/L_s values around this mean value. The sliding-window average can be approximated by the power law

$$\left\langle \frac{L_x}{L_s} \right\rangle = 0.045 \left(\frac{L_s}{10^{28.5}} \right)^{0.23}, \qquad (3)$$

shown by the solid line in Fig. 6.

The width of the shaded region in Fig. 6 indicates that the hardness-luminosity trend described by Eq. (3), which is based on a fairly small sample of sources, should enable ∼50% accuracy for conversion of our soft X-ray luminosity function

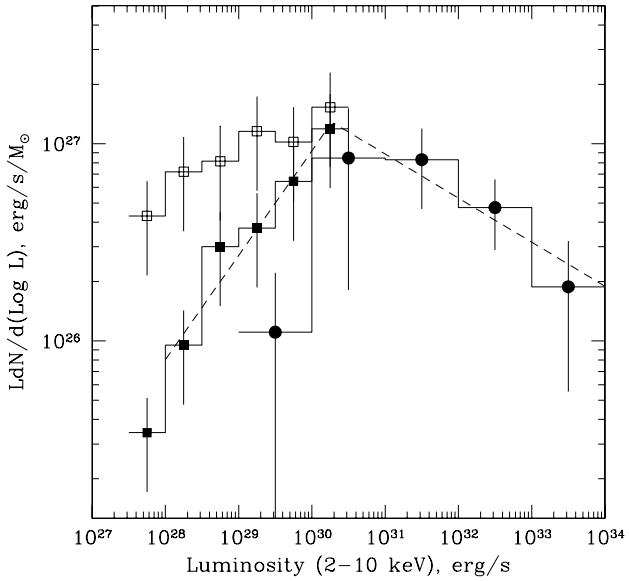

Fig. 7. Differential luminosity distribution of 2–10 keV emissivity per unit stellar mass of coronally active stars and CVs. The XLF derived from the XSS is shown by filled circles, and the XLF derived from the RASS is shown by open squares for all stars and by filled squares for ABs only. The errors shown for the RASS data points take into account an assumed 50% uncertainty of conversion from the original 0.1–2.4 keV band in addition to statistical errors. The dashed line shows the broken power-law fit to the combined XLF of ABs and CVs, given by Eq. (5).

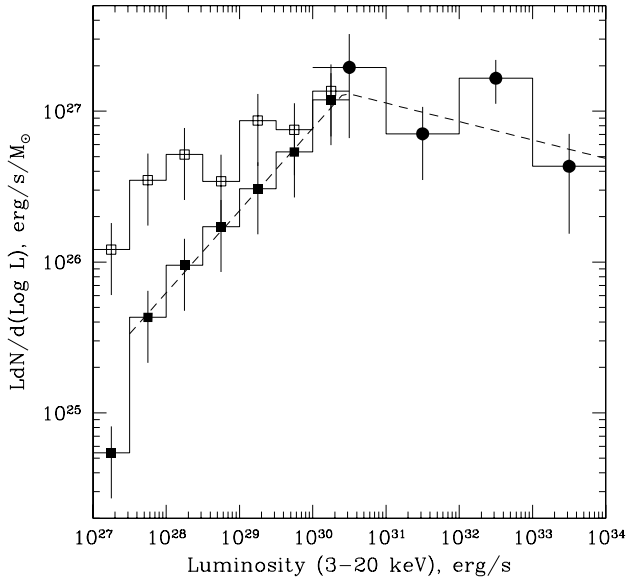

Fig. 8. Same as Fig. 7, but for the 3–20 keV band. The dashed line shows the best-fitting model given by Eq. (6).

(Fig. 5), derived from a much larger sample of RASS sources, to the 2–10 keV energy band for $L_s \gtrsim 10^{28.5}$ erg s^{-1}.

Below we will need a similarly determined approximate trend for the harder energy band 3–20 keV:

$$\left\langle \frac{L_h}{L_s} \right\rangle = 0.02 \left(\frac{L_s}{10^{28.5}} \right)^{0.31} . \quad (4)$$

4. Combined X-ray luminosty function

We then proceeded to convert to a common energy band the X-ray (3–20 keV) and soft X-ray (0.1–2.4 keV) luminosity functions derived from the XSS and RASS in Sects. 2 and 3, respectively. We first considered the 2–10 keV band. For the XSS sample one can readily recompute the XLF using the 2–10 keV source luminosities given in Table 1. We applied a more approximate procedure to the RASS sample, namely converted the measured soft X-ray luminosities to the 2–10 keV range using the approximate hardness-luminosity trend given by Eq. (3) and then recomputed the XLF. The two recomputed XLFs make up a broad range XLF (from $10^{27.5}$ to 10^{34} erg s^{-1}) that is shown in Fig. 7. We then similarly constructed an XLF in the 3–20 keV band (Fig. 8); in this case only the RASS XLF needed to be recomputed using Eq. (4). The 3–20 keV XLF is used by Revnivtsev et al. (2006) to assess the contribution of point sources to the Galactic ridge X-ray emission measured by RXTE in the same energy band.

The XLFs shown in Figs. 7 and 8 were multipled by luminosity to expose the contribution of different luminosity intervals to the total X-ray emissivity per unit stellar mass. In the low-luminosity range covered by RASS data ($L_x < 10^{30.5}$ erg s^{-1}), both the total XLF, including YSs, and separately that of ABs are shown. To roughly allow for the uncertainty of conversion from the original soft X-ray band to the 2–10 keV and 3–20 keV bands we ascribed 50% errors to the RASS data points in addition to statistical uncertainties.

The medium-luminosity XLF derived from the XSS and the low-luminosity XLF derived from the RASS partially overlap near 10^{30} erg s^{-1}, in a region occupied predominantly by ABs, and they do not contradict each other. For the subsequent analysis we adopted the XSS estimates of differential source space densities in the $(10^{30}, 10^{34})$ luminosity range and the RASS estimates of space densities of lower-luminosity sources.

The combined 2–10 keV XLF of ABs and CVs can be approximated in the range 10^{28}–10^{34} erg s^{-1} by a broken power law:

$$\frac{dN}{d\log L_x} = K \begin{cases} (L_b/L_x)^{\alpha_1}, & L_x < L_b \\ (L_b/L_x)^{\alpha_2}, & L_x > L_b, \end{cases} \quad (5)$$

where $K \approx 6.8 \times 10^{-4}\ M_\odot^{-1}$, $L_b \approx 1.9 \times 10^{30}$ erg s^{-1}, $\alpha_1 \approx 0.47$ and $\alpha_2 \approx 1.22$. We note that incompleteness may significantly affect the XLF of ABs below $L_x \sim 10^{28}$ erg s^{-1} (corresponding to $L_s \sim 10^{29.5}$ erg s^{-1}, see Sect. 3) and also somewhat the XLF of CVs above $L_x \sim 10^{31}$ erg s^{-1} (see Sect. 2). Similarly the 3–20 keV XLF of ABs and CVs can be fitted in the range $10^{27.5}$–10^{34} erg s^{-1} by

$$\frac{dN}{d\log L_h} = K \begin{cases} (L_b/L_h)^{\alpha_1}, & L_h < L_b \\ (L_b/L_h)^{\alpha_2}, & L_h > L_b, \end{cases} \quad (6)$$

with $K \approx 4.9 \times 10^{-4}\ M_\odot^{-1}$, $L_b \approx 2.7 \times 10^{30}$ erg s^{-1}, $\alpha_1 \approx 0.45$, and $\alpha_2 \approx 1.12$. These analytical fits (multiplied by luminosity) are shown by dashed lines in Figs. 7 and 8.

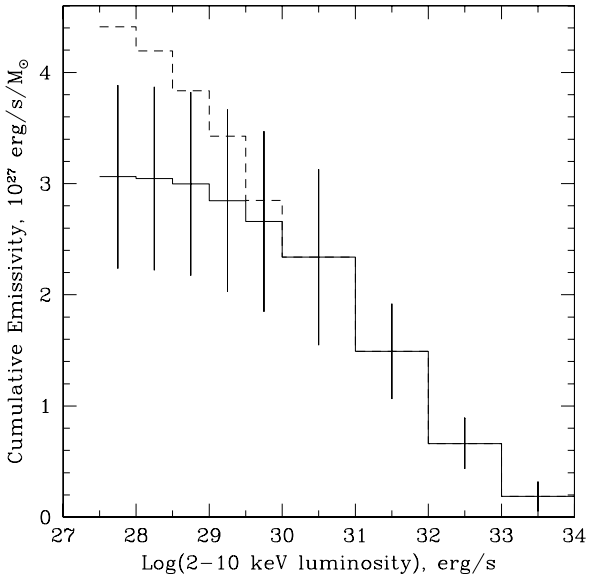

Fig. 9. Cumulative 2–10 keV emissivity of ABs and CVs as a function of luminosity (solid histogram and error bars) and cumulative emissivity of all coronal stars and CVs (dashed histogram). The error bars translate from those for the XLF shown in Fig. 7).

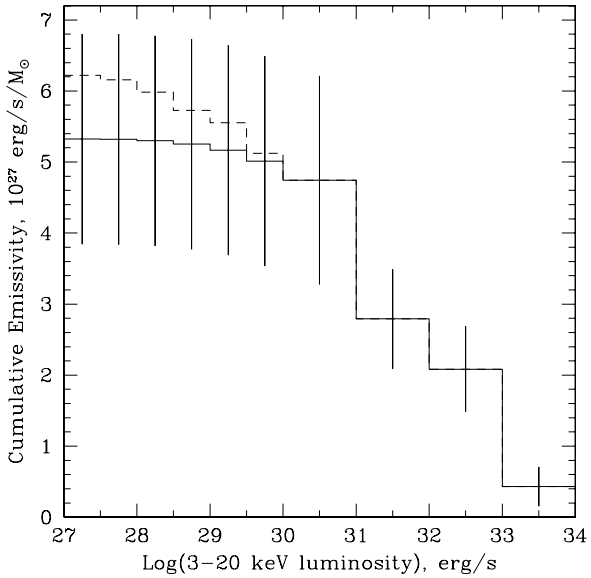

Fig. 10. Same as Fig. 9, but for the 3–20 keV band.

4.1. Cumulative emissivities

Using the differential XLFs obtained above one can assess the cumulative emissivity of local X-ray sources with luminosities below 10^{34} erg s^{-1}. We present in Figs. 9 and 10 the corresponding plots for the 2–10 keV and 3–20 keV bands. Table 4 summarizes our estimates of the cumulative local emissivities (per unit stellar mass) of ABs, CVs, and YSs in the energy bands 0.1–2.4 keV, 2–10 keV and 3–20 keV, complemented by information about LMXBs (see Sect. 4.2 below).

Approximately 80% of the total X-ray (2–10 keV) luminosity of ABs and CVs is produced by sources with $L_{\rm x} > 10^{30}$ erg s^{-1}. In the solar neighborhood an additional significant contribution comes from YSs with $L_{\rm x} \lesssim 10^{30}$ erg $^{-1}$, which make up ∼30% of the total luminosity at 2–10 keV. The fractional contribution of YSs decreases when going to a harder X-ray band because of their relatively soft spectra (compare Figs. 9 and 10). We note that the estimated (by integrating the soft X-ray luminosity function shown in Fig. 5 up to $L_{\rm s} = 10^{32}$ erg s^{-1}) high soft X-ray emissivities of ABs and YSs compared to the harder X-ray bands reflect the fact that stellar coronae are much more efficient sources of soft X-rays than hard X-rays. Also the lower luminosity end of the distributions shown in Figs. 9 and 10 corresponds to $L_{\rm s} \sim 10^{29}$ erg s^{-1}, and the contribution of less luminous X-ray stars (including normal stars like the Sun) to the total X-ray emissivity above 2 keV is expected to be negligible, since they contribute less than 20% to the soft X-ray emissivity and are softer than the more luminous sources (see Sect. 3).

Our preceding analysis does not permit estimation of the soft X-ray emissivity of CVs. The XSS sample is not suitable for this purpose because the high-energy component (optically thin thermal emission with $kT \lesssim 30$ keV) of CV spectra observed by RXTE or a similar X-ray instrument is often intrinsically absorbed below several keV (e.g. Cropper et al. 1998; Suleimanov et al. 2005), while another, much softer component (black-body emission with $kT \sim 30$ eV) appears in the ROSAT energy range, with the relative amplitudes of the two components varying greatly from source to source (Cropper 1990, see also Fig. 3). Therefore, to obtain a reliable estimate of the CV soft X-ray emissivity one has to use a flux-limited and optically identified soft X-ray survey such as the Rosat Bright Survey (RBS, Schwope et al. 2000).

The RBS has already been used by Schwope et al. (2002) to estimate the space density of non-magnetic CVs. Using the same sample of 15 non-magnetic CVs with measured distances (Table 4 in Schwope et al. 2002, which provides source luminosities and $V_{\rm gen}$ values), we can readily estimate the soft X-ray cumulative emissivity (per unit stellar mass) of non-magnetic CVs: $\sim 7 \times 10^{26}$ erg s^{-1}.

Unfortunately, as noted by Schwope et al. (2002), the RBS sample of magnetic CVs suffers substantially from incomplete distance information, which currently makes its use for statistical studies diffucult. Using the published estimate of the space density of magnetic CVs of $\sim 3 \times 10^{-7}$ pc^{-3} (Patterson 1984; Warner 1995), which may be affected by different biases but nevertheless agrees with our XSS based estimate of the space density of magnetic CVs with $L_{\rm x} > 10^{31}$ erg s^{-1} of $(4.8 \pm 1.6) \times 10^{-7}$ pc^{-3}, and assuming $L_{\rm s} \sim 5 \times 10^{31}$ erg s^{-1} for the average source luminosity (e.g. Barrett et al. 1999), we can estimate the soft X-ray emissivity of magnetic CVs at $\sim 4 \times 10^{26}$ erg s^{-1} $M_\odot^{-1}$. Considering that this estimate can be inaccurate by a factor of a few, we infer that the combined soft X-ray emissivity of non-magnetic and magnetic CVs is likely to be less than a few 10^{27} erg s^{-1} $M_\odot^{-1}$. This implies that the total local soft X-ray emissivity is strongly dominated by ABs and YSs (see Table 4).

Table 4. Number densities and emissivities of diffirent classes of sources.

Class	Space density above given luminosity	Total emissivity (10^{27} erg s^{-1} $M_\odot^{-1}$)		
	($M_\odot^{-1}$)	0.1–2.4 keV	2–10 keV	3–20 keV
ABs	$\sim 1.2 \times 10^{-2}$ ($L_x > 10^{27.5}$ erg s^{-1})	(14 ± 4)	2.0 ± 0.8	2.9 ± 1.3
CVs	$(1.2 \pm 0.3) \times 10^{-5}$ ($L_x > 10^{31}$ erg s^{-1})	≲a few	1.1 ± 0.3	2.4 ± 0.6
ABs+CVs		∼15	3.1 ± 0.8	5.3 ± 1.5
YSs		24 ± 3	1.5 ± 0.4	1.0 ± 0.2
ABs+CVs+YSs		∼40	4.5 ± 0.9	6.2 ± 1.5
LMXBs	$\sim 3 \times 10^{-9}$ ($L_x > 10^{36}$ erg s^{-1})	∼40[a]	∼90[b]	

[a] Emissivity in the 0.5–2 keV band extrapolated from 2–10 keV assuming a power-law spectrum of photon index $\Gamma = 1.56$, as typical of LMXBs with 10^{36} erg s^{-1} $< L_x < 10^{39}$ erg s^{-1} (Irwin et al. 2003).
[b] The quoted 2–10 keV emissivity for LMXBs represents an average over nearby galaxies (Gilfanov 2004).

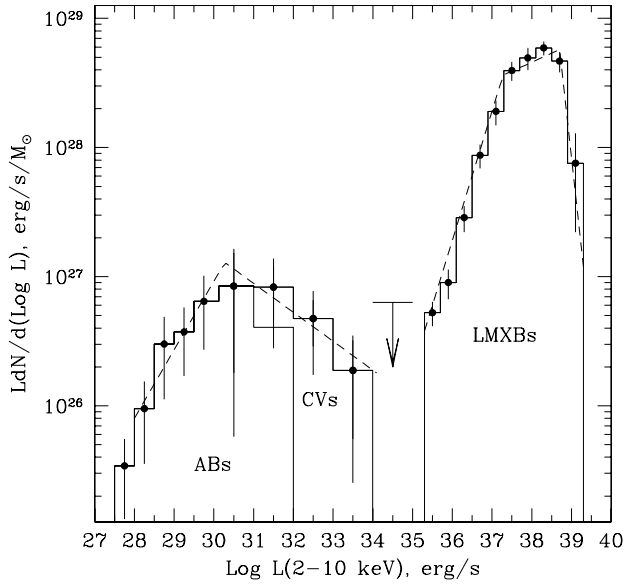

Fig. 11. Differential luminosity distribution of 2–10 keV emissivity of ABs, CVs, and LMXBs. Contributions of these classes of sources are also indicated and analytical approximations given by Eq. (5) and Gilfanov (2004) are presented (dashed lines).

4.2. Addition of LMXBs

The XLF of Galactic LMXBs in the energy band 2–10 keV has been constructed by Grimm et al. (2002). Gilfanov (2004) subsequently demonstrates that the LMXB XLFs for 11 nearby galaxies and the Milky Way have a universal shape and normalizations that are proportional to the stellar masses. We attached the XLF of ABs and CVs constructed here to the XLF of high luminosity LMXBs (∼10^{35}–∼10^{39} erg s^{-1}) averaged over nearby galaxies. The combined XLF (per unit stellar mass) multiplied by luminosity is shown in Fig. 11.

The only poorly studied luminosity interval that remains is 10^{34} to ∼10^{35} erg s^{-1}, but it is possible to place an upper limit on the space density of objects with such luminosities based on the ASCA Galactic Plane Survey (Sugizaki et al. 2001). This survey covers ≈40 sq. deq within the central region of the Galactic plane ($|l| < 45°$ and $|b| < 0.4°$), with the flux limit in the 2–10 keV energy band varying between ∼$10^{-12.5}$ and ∼10^{-12} erg cm^{-2} s^{-1}.

It follows from the number-flux distribution obtained by Sugizaki et al. (2001) that there are on average ∼4 deg^{-2} Galactic sources with flux higher than $10^{-12.5}$ erg cm^{-2} s^{-1} within the region $|l| < 45°$, $|b| < 0.4°$. This implies that the total number of such sources in this region is ∼290. Since the vast majority of weak sources detected in the ASCA survey are unidentified, we can conservatively assume that all detected sources that are brighter than $10^{-12.5}$ erg cm^{-2} s^{-1} have luminosities exceeding 10^{34} erg s^{-1}. At the flux limit of the survey, a source with $L_x > 10^{34}$ erg s^{-1} is detectable out to a distance >16 kpc, i.e. almost to the outer boundary of the Galactic disk. Using the model of stellar mass distribution in the Galactic disk

$$\rho \propto \exp\left[-\left(\frac{R_m}{R}\right)^3 - \frac{R}{R_{scale}} - \frac{z}{z_{scale}}\right], \quad (7)$$

we find that ≈30% of the total mass of the disk is contained within $|l| < 45°$, $|b| < 0.4°$. Here we have assumed $R_m = 3$ kpc, $R_{scale} = 3$ kpc, $R_{max} = 10$ kpc, and $z_{scale} = 150$ pc (Binney et al. 1997; Freudenreich 1998), although the result is almost insensitive to the parameter values except for the scale height z_{scale}. Also taking into account that ∼30% of the Milky Way's stellar mass is contained in the bulge and halo (Bahcall & Soneira 1980; Freudenreich 1998), which are virtually not covered by the ASCA Galactic Plane Survey, we may conservatively estimate that there are less than $290/0.3/(1 - 0.3) \sim 1400$ sources with 10^{34} erg s^{-1} $< L_x < 10^{35}$ erg s^{-1} in the Galaxy. Adopting the value 7×10^{10} $M_\odot$ for the mass of the Galaxy in stars (derived from the K-band luminosity measured by COBE, Malhotra et al. 1996; Gilfanov 2004), we finally obtain the upper limit shown in Fig. 11.

It can be seen from Fig. 11 that the differential luminosity distribution of the X-ray emissivity of Galactic low-mass close binaries has two maxima. The primary peak at $L_x \sim 10^{38}$ erg s^{-1} is due to neutron-star LMXBs accreting at near the Eddington limit. The secondary peak, at ∼10^{29}–10^{33} erg s^{-1}, is formed jointly by ABs and CVs. The XLF can be approximated by Eq. (5) in the range 10^{28}–10^{34} erg s^{-1} and by the LMXB template given in Gilfanov (2004) (their Eqs. (8), (9) and Table 3) in the range 10^{35}–10^{39} erg s^{-1}. Both analytical fits are shown by dashed lines in Fig. 11.

In Fig. 12 we show the cumulative 2–10 keV emissivity of ABs, CVs, and LMXBs as a function of luminosity.

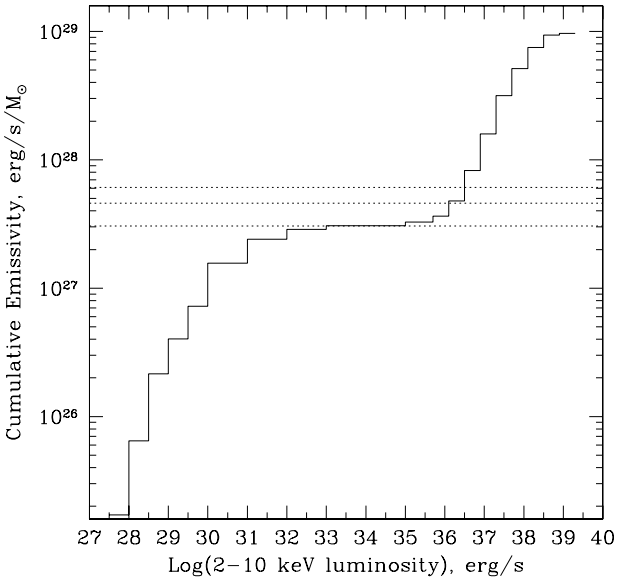

Fig. 12. Cumulative 2–10 keV emissivity (computed from low luminosities upward) of ABs, CVs, and LMXBS as a function of luminosity. The dashed lines show the levels of 100%, 150%, and 200% of the total emissivity of ABs and CVs.

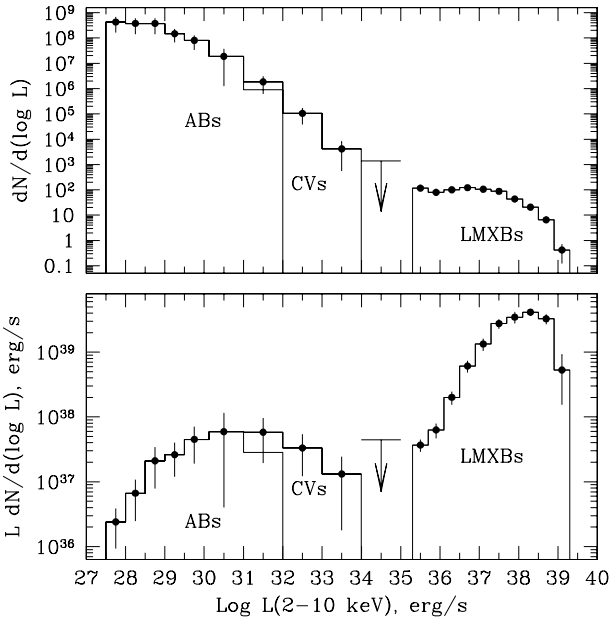

Fig. 13. *Upper panel*: XLF of Galactic low-mass close binaries. The Galaxy stellar mass is assumed to be $7 \times 10^{10}\ M_\odot$ and the LMXB part of the XLF is averaged over nearby galaxies (Gilfanov 2004). *Lower panel*: luminosity distribution of X-ray energy output of Galactic low-mass X-ray binaries.

The LMXBs provide by far the dominant contribution ($\sim 10^{29}$ erg s^{-1} $M_\odot^{-1}$) to the total emissivity, whereas ABs and CVs together contribute ~3%. Figure 12 also demonstrates the effect of cutting out the bright end of the combined XLF: the cumulative emissivity of LMXBs with $L_x < 10^{36}$ ($L_x < 10^{36.5}$) erg s^{-1} is ~50% (~100%) of the total emissivity of ABs and CVs.

Finally Fig. 13 shows the predicted XLF and the luminosity distribution of X-ray energy output of ABs, CVs and LMXBs for the entire Galaxy. The predicted contribution from ABs and CVs to the 2–10 keV luminosity of the Milky Way is $\sim 2 \times 10^{38}$ erg s^{-1}, which agrees within the measurement uncertainties with the total X-ray luminosity of the Galactic ridge X-ray emission (see a detailed discussion in Revnivtsev et al. 2006).

5. Conclusions

In this paper we have constructed the X-ray (above 2 keV) luminosity function of coronally active binaries, CVs, and LMXBs, covering ~12 orders of magnitude in luminosity.

We find that the differential luminosity distribution of X-ray emissivity (per unit stellar mass) of low-mass close binaries has a broad secondary peak at $L_x \sim 10^{29}$–10^{33} erg s^{-1} composed of ABs and CVs, in addition to the previously well-studied primary maximum at $\sim 10^{38}$ erg s^{-1} made up of neutron-star LMXBs accreting near the Eddington limit. The combined emissivity of ABs and CVs in the 2–10 keV band is $(3.1 \pm 0.8) \times 10^{27}$ erg s^{-1} $M_\odot^{-1}$, or ~3% of the emissivity of LMXBs (averaged over nearby galaxies). About 65% of this total emissivity is due to ABs. The estimated combined contribution of ABs and CVs to the 2–10 keV luminosity of the Milky Way is $\sim 2 \times 10^{38}$ erg s^{-1}.

Young coronal stars with luminosities $L_x \lesssim 10^{30}$ erg s^{-1} provide an additional significant contribution of $(1.5 \pm 0.4) \times 10^{27}$ erg s^{-1} $M_\odot^{-1}$ to the cumulative 2–10 keV emissivity in the solar neighborhood (within ~50 pc). However, the fractional contribution of YSs to the X-ray emissivity is expected to vary substantially across the Galaxy, reflecting local star formation history. In contrast, the cumulative X-ray emission of ABs and CVs is expected to approximately follow the distribution of stellar mass, as is known to be the case for LMXBs.

The results of this work find immediate application to the problem of the origin of Galactic ridge X-ray emission. Revnivtsev et al. (2006) use the XLF constructed here in combination with the X-ray surface brightness distribution of the ridge emission, which is shown to follow the stellar mass, to demonstrate that ABs and CVs (with a possible contribution from YSs) probably produce the bulk of the ridge emission.

The results of this work also indicate that in order to assess the contribution of low-luminosity point X-ray sources (ABs and CVs) to the apparently diffuse X-ray emission of gas-poor elliptical galaxies, it is necessary to resolve the brightest LMXBs with $L_x \gtrsim 10^{36}$ erg s^{-1} (see Fig. 12). This can already be achieved with Chandra for nearby galaxies. It should be taken into account, however, that in elliptical galaxies a significant fraction of low-mass close binaries reside in globular clusters where their numbers are expected to be affected by dynamical processes in combination with aging (e.g. Verbunt & Lewin 2005). It will be important to compare the XLF derived here for the solar neighborhood in future work with that determined for Galactic globular clusters from deep Chandra observations (e.g. Heinke et al. 2005).

Acknowledgements. This research has made use of the SIMBAD database (operated at the CDS, Strasbourg) and the High Energy Astrophysics Science Archive Research Center Online Service provided by the NASA/Goddard Space Flight Center.

References

Araujo-Betancor, S., Gänsicke, B. T., Long, K. S., et al. 2005, ApJ, 622, 589
Bahcall, J. N., & Soneira, R. M. 1980, ApJS, 44, 73
Barrett, P., Singh, K. P., & Mitchell, S. 1999, Annapolis Workshop on Magnetic Cataclysmic Variables, ASP Conf. Ser., 157, 180
Baskill, D. S., Wheatley, P. J., & Osborne, J. P. 2005, MNRAS, 357, 626
Beuermann, K., Harrison, Th. E., McArthur, B. E., et al. 2004, A&A, 419, 291
Binney, J., Gerhard, O., & Spergel, D. 1997, MNRAS, 288, 365
Canizares, C. R., Fabbiano, G., & Trinchieri, G. 1987, ApJ, 312, 503
Cropper, M. 1990, SSRv, 54, 195
Cropper, M., Ramsay, G., & Wu, K. 1998, MNRAS, 293, 222
Dempsey, R. C., Linsky, J. L., Schmitt, J. H. M. M., & Fleming, T. A. 1993, ApJ, 413, 333
Ebisawa, K., Tsujimoto, M., Paizis, A., et al. 2005, ApJ, 635, 214
Eisenbart, S., Beuermann, K., Reinsch, K., & Gänsicke, B. T. 2002, A&A, 382, 984
Fleming, T. A., Gioia, I. M., & Maccacaro, T. 1989, AJ, 98, 692
Fleming, T. A., Molendi, S., Maccacaro, T., & Wolter, A. 1995, ApJS, 99, 701
Freudenreich, H. T. 1998, ApJ, 492, 495
Gänsicke, B. T., Marsh, T. R., Edge, A., et al. 2005, MNRAS, 361, 141
Gilfanov, M. 2004, MNRAS, 349, 146
Gliese, W., & Jahreiß, H. 1991, Preliminary version of the Third Catalog of Nearby Stars, on: The Astronomical Data Center CD-ROM: Selected Astronomical Catalogs, Vol. I, ed. L. E. Brotzmann, & S. E. Gesser, NASA/Astronomical Data Center, Goddard Space Flight Center, Greenbelt
Grimm, H.-J., Gilfanov, M., & Sunyaev, R. 2002, A&A, 391, 923
Güdel, M. 2004, A&ARv, 12, 71
Hands, A. D. P., Warwick, R. S., Watson, M. G., & Helfand, D. J. 2004, MNRAS, 351, 31
Hearty, T., Neuhäuser, R., Stelzer, B., et al. 2000, A&A, 353, 1044
Heinke, C. O., Grindlay, J. E., Edmonds, P. D., et al. 2005, ApJ, 625, 796
Hessman, F. V. 1998, A&AS, 72, 515
Hünsch, M., Schmitt, J. H. M. M., Sterzik, M. F., & Voges, W. 1999, A&AS, 135, 319 (H99)
Irwin, J. A., Athney, A. E., & Bregman, J. N. 2003, ApJ, 587, 356
Jahreiß, H., & Wielen, R. 1997, Hipparcos '97, ed. B. Battrick, M. A. C. Perryman, & P. L. Bernacca, ESA SP-402, 675
Karataş, Y., Bilir, S., Eker, Z., & Demircan, O. 2004, MNRAS, 349, 1069
Littlefair, S. P., Dhillon, V. S., & Marsh, T. R. 2001, MNRAS, 327, 669
Makarov, V. 2003, ApJ, 126, 1996 (M03)
Malhotra, S., Spergel, D. N., Rhoads, J. E., & Li, J. 1996, ApJ, 473, 687
Matsumoto, H., Koyama, K., Awaki, H., et al. 1997, ApJ, 482, 133
McArthur, B. E., Benedict, G. F., Lee, J., et al. 2001, ApJ, 560, 907
Mukai, K., & Shiokawa, K. 1993, ApJ, 418, 863
Muno, M. P., Baganoff, F. K., Bautz, M. W., et al. 2004, ApJ, 613, 326
Ottmann, R., & Schmitt, J. H. M. M. 1992, A&A, 256, 421
Patterson, J. 1984, ApJS, 54, 443
Patterson, J. 1994, PASP, 106, 209
Revnivtsev, M., Sazonov, S., Jahoda, K., & Gilfanov, M. 2004, A&A, 418, 927 (R04)
Revnivtsev, M., Sazonov, S., Gilfanov, M., Churazov, E., & Sunyaev, R. 2006, A&A, in press
Robin, A. C., Reylé, C., Derrière, & Picaud, S. 2003, A&A, 409, 523
Samus, N. N., Durlevich, O. V., et al. 2004, Combined General Catalogue of Variable Stars, VizieR On-line Data Catalog: II/250
Sazonov, S. Y., & Revnivtsev, M. G. 2004, A&A, 423, 469
Schmidt, M. 1968, ApJ, 151, 393
Schmitt, J. H. M. M., Collura, A., Sciortino, S., et al. 1990, ApJ, 365, 704
Schwope, A. D., Hasinger, G., & Lehmann, I. 2000, AN, 321, 1
Schwope, A. D., Brunner, H., Buckley, D., et al. 2002, A&A, 396, 895
Silber, A. D., Remillard, R. A., Horne, K., & Bradt, H. V. 1994, ApJ, 424, 955
Singh, K. P., Drake, S. A., & White, N. E. 1996, AJ, 111, 2415
Smith, D. A., & Dhillon, V. S. 1998, MNRAS, 301, 767
Sokoloski, J. L., & Kenyon, S. J. 2003, ApJ, 584, 1021
Strassmeier, K. G., Hall, D. S., Fekel, F. C., & Scheck, M. 1993, A&AS, 100, 173
Sugizaki, M., Mitsuda, K., Kaneda, H., et al. 2001, ApJS, 134, 77
Suleimanov, V., Revnivtsev, M., & Ritter, H. 2005, A&A, 435, 191
Tinney, C. G., Reid, I. N., & Mould, J. R. 1993, ApJ, 414, 254
Thorstensen, J. R. 2003, AJ, 126, 3017
Tovmassian, G. H., Greiner, J., Kroll, P., et al. 1998, A&A, 335, 227
Verbunt, F., & Lewin, W. H. G. 2005, in Compact Stellar X-ray Sources, ed. W. H. G. Lewin, & M. van der Klis, in press (Cambridge University Press) [arXiv:astro-ph/0404136]
Voges, W., Aschenbach, B., Boller, Th., et al. 1999, A&A, 349, 389
Warner, B. 1995, Cataclysmic variable stars, Cambridge Astrophysics Series (Cambridge University Press)
Warwick, R. S., Turner, M. J. L., Watson, M. G., & Willingale, R. 1985, Nature, 317, 218
Worrall, D. M., & Marshall, F. E. 1983, ApJ, 267, 691
Worrall, D. M., Marshall, F. E., Boldt, E. A., & Swank, J. H. 1982, ApJ, 255, 111